Journal of Hazardous Materials 183 (2010) 301–308

Contents lists available at ScienceDirect

Journal of Hazardous Materials

journal homepage: www.elsevier.com/locate/jhazmat

Solid phase studies and geochemical modelling of low-cost permeable reactive barriers

Georgios Bartzas[a,*], Kostas Komnitsas[b]

[a] Laboratory of Metallurgy, School of Mining and Metallurgical Engineering, National Technical University of Athens, Zografos Campus, 15780 Athens, Greece
[b] Department of Mineral Resources Engineering, Technical University of Crete, 73100 Chania, Greece

ARTICLE INFO

Article history:
Received 28 January 2010
Received in revised form 17 May 2010
Accepted 8 July 2010
Available online 15 July 2010

Keywords:
Acid mine drainage
Geochemical modelling
Permeable reactive barrier
Zero-valent iron

ABSTRACT

A continuous column experiment was carried out under dynamic flow conditions in order to study the efficiency of low-cost permeable reactive barriers (PRBs) to remove several inorganic contaminants from acidic solutions. A 50:50 w/w waste iron/sand mixture was used as candidate reactive media in order to activate precipitation and promote sorption and reduction–oxidation mechanisms. Solid phase studies of the exhausted reactive products after column shutdown, using scanning electron microscopy (SEM), Fourier transform infrared spectroscopy (FTIR) and X-ray diffraction (XRD), confirmed that the principal Fe corrosion products identified in the reactive zone are amorphous iron (hydr)oxides (maghemite/magnetite and goethite), intermediate products (sulfate green rust), and amorphous metal sulfides such as amFeS and/or mackinawite. Geochemical modelling of the metal removal processes, including interactions between reactive media, heavy metal ions and sulfates, and interpretation of the ionic profiles was also carried out by using the speciation/mass transfer computer code PHREEQC-2 and the WATEQ4F database. Mineralogical characterization studies as well as geochemical modelling calculations also indicate that the effect of sulfate and silica sand on the efficiency of the reactive zone should be considered carefully during design and operation of low-cost field PRBs.

1. Introduction

Acid mine drainage (AMD) occurs when reactive sulfide minerals (e.g. pyrite) are exposed to oxygen and water in the absence of sufficient neutralizing minerals. These leachates, characterized by low pH and high concentrations of SO_4^{2-}, Fe and several toxic metals, are responsible for the deterioration of the quality of surface- and groundwater as well as soils [1].

In recent years, attention has been paid to the use of permeable reactive barriers (PRBs) for the clean-up of acidic plumes and the prevention of groundwater contamination. PRBs comprise an engineered treatment zone of reactive material(s) that is placed in the subsurface in order to remediate a contaminated groundwater plume as it flows through [2]. The contaminants are removed from groundwater by transformation to less dangerous compounds and/or efficient removal by the reactive material. The key element for the design and efficient in situ operation of a PRB system is the selection of an appropriate reactive medium, which, depending on the type of the contaminant, should be characterized by increased reactivity, sufficient permeability or hydraulic conductivity, excellent environmental compatibility, availability, low-cost, and long-term stability.

Commercial zero-valent iron (Fe^0) has been used as reactive material in most constructed PRBs to degrade organic pollutants. Chemical reduction by zero-valent iron has been extensively studied for the treatment of chlorinated organics, nitroaromatic compounds and pesticides [3]. Recently, due to its strong reducing capacity and ability to alter its valence state into more favourable forms for sorption and reductive precipitation, commercially available iron has been also successfully used for the remediation of AMD contaminated by a large number of metals and trace elements such as As, Cd, Co, Cr, Hg, Ni, Se, U and Zn [4]. Furthermore, due to the continuous oxidation of zero valent iron in PRB systems, a substrate of iron oxides is formed enhancing thus sorption of several contaminants [5,6]. Nevertheless, the relatively high cost of commercial Fe^0 fillings may prevent their use at small contaminated sites especially in developing countries.

As a result, laboratory attempts using industrial wastes or by-products from other metallurgical or chemical processes such as fly ash, bottom ash and red mud as potential cost-effective and convenient sorbents for the removal of heavy metals have been recently performed [7–9]. Waste iron in the form of steel scrap or iron sludge seems to be a good alternative, as it is either discarded or sold at very low prices (20 times lower than commercial iron) depending

* Corresponding author. Tel.: +30 210 772 2181; fax: +30 210 772 2218.
E-mail address: gbartzas@metal.ntua.gr (G. Bartzas).

0304-3894/$ – see front matter © 2010 Elsevier B.V. All rights reserved.
doi:10.1016/j.jhazmat.2010.07.024

on its reactive content characteristics. Indeed, in most cases waste iron contains high amounts of Fe^0 which are directly available for the treatment of contaminants without the need of any pretreatment. These waste materials, as a result of the treatment process, are usually covered with a double layer of iron oxides; however, previous studies showed that when placed in acidic solutions, the outer passive oxide layer is removed or converted by autoreduction to a conducting magnetite film [10–13].

Despite the extensive field iron PRB applications, there is still much uncertainty in predicting their long-term effectiveness and hydraulic performance over long periods of time as well as the type of precipitates formed under given conditions. In most cases, the metal removal mechanisms by Fe^0 are not well defined/understood but are believed to involve cementation, adsorption and reductive mineral precipitation processes. However, the predominant inorganic contaminant removal pathway is generally favoured by iron corrosion depending on the metal species and experimental conditions. Previous studies have shown that the main corrosion product is amorphous ferrous hydroxide, which can be thermodynamically converted to non-stoichiometric magnetite (Fe_3O_4) [14] or to other intermediate products known as green rusts [$GR(SO_4^{2-})$] [11,14]. Secondary reactions cause the formation of magnetite, maghemite (γ-Fe_3O_4), goethite (a-FeOOH) and lepidocrocite (γ-FeOOH) [16,17]. The type of the secondary minerals is primarily dependent on the solution chemistry and the prevailing flow conditions.

As a result of these oxidation–reduction reactions, the Fe^0 surface is gradually coated by a layer of iron oxides and oxyhydroxides and therefore the effective porosity of the reactive medium is reduced. In many studies, strong emphasis has been recently laid on mixing zero-valent iron with sand to reduce material costs [18], prevent loss of reactivity and hydraulic conductivity and in turn avoid reduction of groundwater flow [19,20]. Addition of sand increases accessible porosity and eliminates both pore clogging and development of preferential flow channels by creating connected pores not subject to infilling by corrosion products such as oxides [13,21]. However, several issues related to interfacial reactions of Fe^0 and its corrosion products with silicon substrates during treatment require further elucidation.

Solid phase investigations coupled with geochemical studies of the exhausted reactive media can be used to further predict mineral precipitation and pore clogging changes and subsequently evaluate their effect on reactive materials hydraulic and treatment efficiency [22,23]. Solid phase studies can accurately assess the extent of iron corrosion, the role of the presence of potential buffering minerals and the effect of precipitation of secondary minerals on reactive sites. In addition, mobilisation and removal of metals can be evaluated with aqueous sampling and determination of pore water chemistry. Reactive transport modelling is another valuable tool that can be used for the elucidation of the mechanisms involved in each reactive system and the prediction of the effective lifetime especially in field applications. Its use is extremely important during evaluation of complicated multi-component systems such as AMD contaminated waters. A combination of these approaches provides valuable information on physical and chemical alterations in the reactive zone and assists in the design of iron PRBs as a viable long-term and cost-effective remediation technology.

In the present study, a long-term continuous column experiment was carried out using a mixture of waste iron and sand as reactive material to study the clean-up of acidic leachates and assess the effect of sulfate ions and mineral precipitation on iron corrosion. Solid phase studies using XRD, SEM and FTIR coupled with geochemical modelling calculations were used to investigate the formation of new mineral phases and identify iron corrosion products. Emphasis was laid on the evaluation of the effect of silica sand as admixing material on the performance and longevity of waste iron-based PRBs during field treatment of acidic leachates.

2. Materials and methods

2.1. Materials

2.1.1. Waste iron

Waste iron filings (0.2–1.2 mm) were obtained from Gotthart Maier, Germany, and used as received. They have irregular shape and slightly rough surface, while they contain 92% elemental iron, approximately 3.3% carbon, and minor impurities. Their specific surface area as determined by the BET N_2-method was 0.0482 m^2/g.

2.1.2. Silica sand

Silica sand (0.2–1.0 mm) was collected from a coastal area of Milos Island, Greece. Its chemical analysis using XRF revealed the presence of 97% SiO_2 and traces of aluminum and sodium oxides; no iron oxides were detected. Prior to use, sand particles were soaked in 8% v/v HNO_3 for 24 h and then rinsed with deionized water.

2.2. Experimental set-up

The experimental procedure (design, column set-up and operation) has been described in detail in an earlier publication [24]. Briefly, two plexiglas columns (45 cm length, 5 cm internal diameter) were used in a series. Each column was homogeneously packed with a 40 cm layer of 50:50 w/w waste iron filings/silica sand while two 2.5 cm layers of silica sand were places at both ends. The porosity of the packed waste iron/sand zone was calculated by weight difference after filling the column with distilled water and confirmed by a tracer test (55%); a non-reactive chloride was flushed into the column and the breakthrough of the tracer front was determined at the effluent sampling port. The experimental data were modelled using the one-dimensional advection-dispersion equation so that an identical porosity was derived.

The upflow column test was performed at constant temperature, 25 ± 2 °C. An artificial acidic solution comprising several metal sulfates was prepared from concentrated stock analytical grade solutions to simulate the chemical composition of typical AMD generated in most mining and waste disposal sites (Table 1). No iron was added because a) its concentration in real solutions is usually much higher than the concentration of the other elements, dominating thus system kinetics and formation of new phases, and b) iron is released in the system due to the corrosion of Fe^0. No further pH adjustment of the incoming feed was required as its natural acidity (pH 1.8) prevents precipitation of metal phases. All chemicals used were reagent grade (Merck, Aldrich or Fluka).

Upward flow of the simulated AMD feed was applied using a peristaltic pump Gala/4W in order to precisely simulate typical groundwater flow rate of approximately 152.4 cm/day (~5 ft/day)

Table 1
Feed solution composition and corresponding chemicals used.

Contaminants	Concentration in mg/L	Used chemicals
Al^{3+}	500	$Al_2(SO_4)_3{\cdot}18H_2O$
Zn^{2+}	100	$ZnSO_4{\cdot}7H_2O$
Cd^{2+}	25	$3CdSO_4{\cdot}8H_2O$
Cu^{2+}	50	$CuSO_4{\cdot}5H_2O$
Mn^{2+}	50	$MnSO_4{\cdot}H_2O$
Ni^{2+}	50	$NiSO_4{\cdot}6H_2O$
Co^{2+}	50	$CoSO_4{\cdot}7H_2O$
SO_4^{2-}	5840	–
pH	1.8	

and eliminate channelling and gas entrainment. Before running the tests at steady flow conditions, three pore volumes of distilled water were flushed through the columns to equilibrate the system and remove residual oxygen from the voids. All tests were carried out in duplicate.

2.3. Solid sample extraction and preparation

After completion of the tests, the columns were brought into an anaerobic chamber and samples were extracted to perform solid phase characterization studies. Solid samples of "exhausted" reactive material (approximately 30 g) were taken from 3 representative sampling points (bottom, middle and top of the column) under nitrogen atmosphere to minimize oxidation and washed gently with deoxygenated acetone/water solution (1:1 volume ratio).

Prior to mineralogical analysis, all samples were gently ground using an agate mortar and pestle and then sieved manually. This procedure enabled separation of coarse particles (>140 μm, mostly Fe^0 filings) from the fine exhausted material (fractions of <63 and 63–140 μm, mainly precipitated minerals and fine Fe^0 filing fragments) and adequate removal of precipitates. This procedure is suitable when unstable minerals precipitate and wide assortment of mineralogy appears due to gradual iron corrosion. The coarse fraction (>140 μm) was hand ground and sieved two more times in order to adequately remove surface precipitates.

2.4. Solid phase studies

2.4.1. XRD and FTIR

The mineralogical composition of column precipitates was determined by X-ray powder diffraction (XRD) and Fourier transform infrared spectroscopy (FTIR). Copper Kα radiation and a Bruker D8 Focus diffractometer equipped with a vertical goniometer and a curved Cu diffracted beam monochromator was used in XRD studies. Samples were scanned from 2 to 70° 2θ with 0.02° step and a counting rate of 1 s/step. FTIR spectra were derived using a Perkin–Elmer/Spectrum 100 spectrometer, in the range between 400 and 4000 cm^{-1}. An 8 mg sample was mixed with 300 mg of KBr and pellets were obtained after pressing the mixture.

2.4.2. SEM

Scanning electron microscopy (SEM) and energy dispersive X-ray spectroscopy (EDS) were used to evaluate the morphology and composition of precipitates formed on the surface of the zero-valent iron/sand particles. Measurements were conducted on polished sections to determine the composition of surface precipitates on a semi-quantitative basis. Samples for SEM and EDS analysis were stored in an anaerobic glove box and then embedded in an epoxy resin. Prior to SEM analysis, the epoxy-embedded samples were polished using diamond abrasives and then coated with a thin gold layer. Secondary electron and back-scattered electron images were obtained using a JEOL-6380LV (Tokyo, Japan). The instrument was operated using a 20 kV electron accelerating potential and a beam current of about 10 nA.

2.5. Geochemical modelling

The main reactions taking place in the reactive zone were simulated using the PHREEQC version 2 software for speciation and one-dimensional transport [25]. The PHREEQC-2 code enables calculation of mineral saturation indices and allows prediction of mineral precipitation that potentially controls the composition of the aqueous phase during column operation. Thermodynamic constants were retrieved from the WATEQ4F database [26].

3. Results and discussion

During the continuous operation of the column system over a period of nearly 1.5 months, physical and chemical changes were observed. At the end of the runs, visible changes in the colour of the reactive mixture from slight reddish (Fe^{3+} hydroxide) to greyish green (Fe^{2+} hydroxide) were seen in the lower parts of the system.

The contaminant removal performance of waste iron/sand column system has been evaluated in detail in an earlier study [22]. An oxide film was gradually formed due to the oxidation of zero-valent iron, covered its surface and subsequently reduced the overall reactivity of the system. As a result, porosity in the iron packed columns during steady-state AMD clean-up decreased from the initial value of 0.55–0.39; this value indicates that residence time is decreased by four times. In order to determine the degree of iron corrosion and further elucidate the removal mechanisms involved, newly formed precipitates and iron corrosion products were characterized by surface and structure analyses.

3.1. Iron corrosion products – effect of sulfates on metal removal

When the acidic solution reacts with the iron fillings, iron corrosion takes place and pH increases (Eq. (1)):

$$4Fe^0 + 8H_2O \Rightarrow 4Fe^{2+} + 8OH^- + 4H_2 \quad (1)$$

As a result of this reaction, the effluent pH increased at the early stages of the experiment to 8.5; this is a typical value for iron systems operating under moderate acidity and concentration of contaminant. The rate of iron corrosion is controlled by the number of sulfate ions present in the feed.

XRD analyses of the <63 μm fraction of precipitates formed at the lower part of the system showed that apart from sand, the main crystalline phases were sulfate green rust, goethite, and magnetite (Fe_3O_4)/maghemite (γ-Fe_2O_3) (Fig. 1). The last two mineral phases are normally difficult to be distinguished by XRD, as they exhibit similar XRD patterns differing in spacing by about 0.47% [27]. Under slightly acidic conditions seen in this study, magnetite can contain excessive amounts of maghemite or can be totally transformed to its related product. As no significant mass of iron oxides is seen in the unreacted iron particles, it is believed that their formation was entirely due to Fe^0 corrosion. Substantial amounts of both magnetite and maghemite have been detected in the reactive zone of iron PRBs operating in the field.

$Fe(OH)_2$ and ferrihydrite ($Fe_5OH_8{\cdot}4H_2O$) are usually the first iron corrosion products. Although ferrihydrite has been detected by transmission electron microscopy in PRBs containing commercial iron [28], its formation was not identified by XRD in the present study. Thermodynamic modelling calculations performed with PHREEQC-2 at the given experimental conditions in the iron/sand system, indicated that at acidic pH the reactive zone was undersaturated in terms of ferrihydrite formation and oversaturated in terms of both magnetite and hematite precipitation.

The XRD pattern of the precipitates formed indicated also the presence of elemental copper, a redox-active phase formed by the reduction of dissolved copper and its subsequent deposition onto the iron surface. The removal mechanism for copper ions by zero-valent iron (cementation) ($E^{\theta}_{Fe^{2+}/Fe} = -0.44\,V$, $E^{\theta}_{Cu^{2+}/Cu} = 0.34\,V$) is discussed extensively in a previous study [24] and is briefly described here by the following redox equation:

$$Fe^0 + Cu^{2+} \Rightarrow Fe^{2+} + Cu^0 \quad (2)$$

Although, the ability to detect amorphous and metastable mineral phases by powder XRD is limited due to indirect inference, instrument-related intensity variations and orientation effects, solid sampling and preparation procedure used in this study

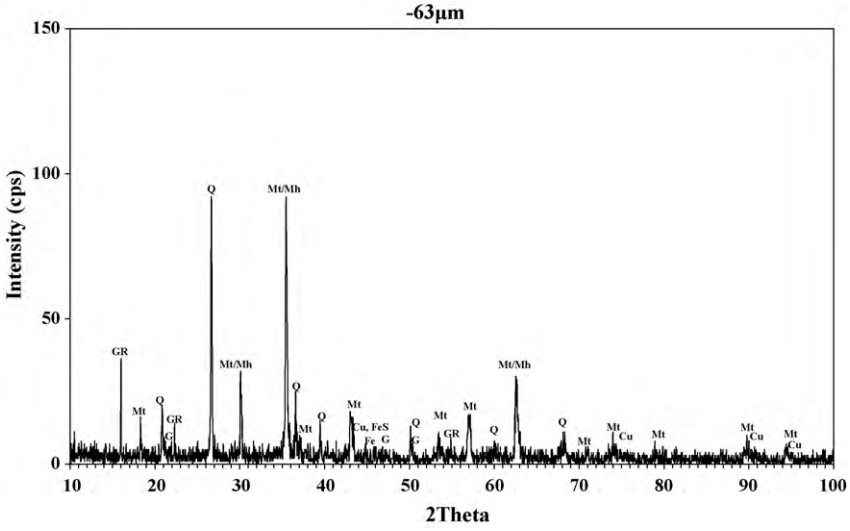

Fig. 1. X-ray pattern of precipitates in the <63 μm fraction collected from the lower part of the column system. Fe, zero-valent iron; GR, sulfate green rust; G, goethite; FeS, iron sulfide; Mt/Mh, maghemite and/or magnetite; Q, quartz; and Cu, elemental copper.

enabled the XRD detection of amorphous iron sulfide [(am)FeS]. Previous studies [12,15] have shown that sulfate behaves as a stronger reducing agent than the corresponding aqueous species present in solution and it could be responsible for the precipitation of iron sulfides, as seen in the following reactions:

$$4Fe^0 + 8H_2O \Rightarrow 4Fe^{2+} + 8OH^- + 4H_2 \quad (3)$$

$$SO_4^{2-} + 4H_2 \Rightarrow HS^- + 3H_2O + OH^- \quad (4)$$

$$4Fe^{2+} + HS^- + 7OH^- \Rightarrow FeS(am) + 3Fe(OH)_2(am) + H_2O \quad (5)$$

The reduction of sulfate to sulfide occurs in natural AMD systems at pH values as low as 2–3 [29,30]. However, mineralogical investigations in field iron PRBs showed that microbial activity is an important promoter of sulfate reduction and subsequent precipitation of am FeS. Amorphous iron sulfide can be disordered/transformed to mackinawite [$Fe_{(1+x)}S$] [31], a mineral phase that can present high metal removal capacity even at low pH [32].

The presence of significant amounts of sulfate in the simulated AMD feed (5840 mg/L) increases the likelihood for heavy metal co-precipitation by the formation of ternary metal-sulfate surface complexes. On the contrary, S^- does not tend to react with metal ions and form metal sulfide complexes but may compete with sulfates for adsorption sites and hence inhibit metal adsorption.

Geochemical modelling with PHREEQC-2 also confirms that the major contribution to iron corrosion is due to sulfate reduction. However, sulfate can be easily removed from solution by precipitation as metal sulfur compound, e.g., metal-sulfate/hydroxide complexes. Sulfate is also known to adsorb on iron (oxy)hydroxide surfaces such as goethite and maghemite exhibiting net positive charge at low pH [33]. Nevertheless, this behaviour may inhibit metal removal as the presence of SO_4^{2-} slows down the transformation of primary iron hydroxides into more crystallized and reactive oxides [31].

It is believed that dissolved Al may also inhibit iron corrosion in near neutral pH conditions when the effluent solution is below saturation with respect to AlOOH [19]. However, geochemical calculations carried out in this study predict that aluminium concentration in the PRB is mainly controlled by the formation of amorphous $Al(OH)_3$ or jurbanite ($AlOHSO_4{\cdot}5H_2O$) when pH is above or below 5.5 respectively. This is supported by the relatively low sulfate concentration (475 mg/L) recorded at the final effluent as well as by previous studies [12,34].

The nature of the surface groups present in the reacted iron particles was further investigated with FTIR (Fig. 2). The spectra of the precipitated fines (<63 μm fraction) separated from the corroded waste iron filings consist of three main regions of interest: the O–H stretching region from 4000 to 2000 cm^{-1}, the combination band and overtone region from 2000 to 1200 cm^{-1}, and the lattice mode and molecular ion region from ca. 1200 to 400 cm^{-1} [35].

It is important to note that FTIR analysis did not show the characteristic spectral bands of surface silanols SiOH elongations of pure quartz in the area 3600–3800 cm^{-1}, as a result of its bonding with hydrogen, either intramolecularly or with absorbed water. This phenomenon may let us assume that these hydrogen based elongations disappeared in the profit of the connections SiOFe in the coated reactive mixture. In fact, the bands centred at 430 and 490 cm^{-1} confirmed the presence of SiOFe bond [36].

The lattice mode is the most complex region to determine in the spectra of the mixed corrosion products. The peaks around 476 and 1120 cm^{-1} observed for corrosion products in the exhausted reactive mixture correspond to the bending and stretching vibrations of Fe–O bonding, indicating the existence of iron (hydr)oxides precipitates. The typical bands of α-FeOOH at 890 and 798 cm^{-1} are the most noticeable features of spectra. The IR pattern of magnetite is also present in iron corroded samples, showing a broad band at 575 cm^{-1} and a very broad band of low intensity at 408 cm^{-1} [37].

FTIR studies fully confirmed the formation of sulfate green rust and maghemite under the particular conditions of this column experiment. The IR spectrum of GR (SO_4^{2-}) is well known [38] and it is characterized by two main peaks at around (618–668) and (1100–1138) cm^{-1}. Respectively, the very broad and poor resolved feature near 1400 cm^{-1} is also characteristic of maghemite [39]. Both these peaks observed on the exhausted iron samples indicate that the IR data are, as a whole, consistent with the XRD analyses. Finally, absorption bands at 610 and 778 cm^{-1} are related to stretching modes of sulfates in association with a metal ion such as aluminium or iron [40,41]. Under the given experimental conditions, those absorption bands indicate the formation of the corresponding sulfates or their hydrated forms.

SEM images and EDS analyses were also used to examine the morphology of the newly formed precipitates and iron corrosion products as well as their elemental composition. Microscopic characterization of the reacted iron/sand material indicates that within the reactive zone mineral accumulation does not only occur on the surface of iron grains but also in the form of free mineral precip-

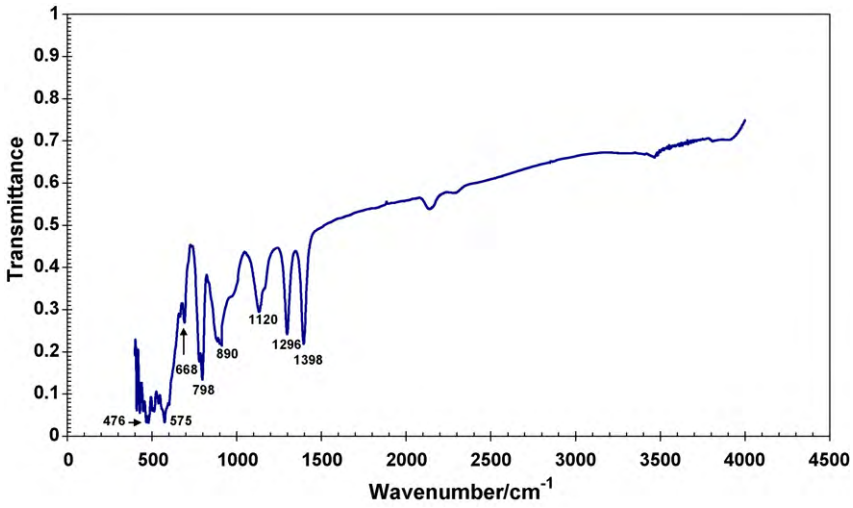

Fig. 2. FTIR spectra of iron corrosion products.

itates not directly attached to iron grains. As seen in Fig. 3, the iron grain (brighter area) is coated with a nearly compact phase comprising three distinct layers: an outer thick shell, a middle crystalline layer and an inner fibrous layer of small needles or plates adjacent to iron metal surface. The iron reactive area is brighter in the SEM image because iron atoms when bombarded by high energy electrons emit more secondary electrons than epoxy molecules do, so that more electrons are collected by the detector.

The presence of the oxygen peak on the SEM-EDS images, ranging from 6.96% (Fig. 3b) to 30.92% w/w (Fig. 3c), provides a clear evidence that the formation of both oxides, magnetite (Fe_3O_4) and maghemite (Fe_2O_3), dominates the coating shell that was created at the Fe^0/solution interface. Coatings on iron grains are in some regions either thin (20 μm) or over 100 μm filling thus completely pore spaces.

The occurrence and predominance of the mineral phases vary along the flow-path length and the proximity to the sand–Fe^0 interface, fundamentally reflecting the significance of the pore water chemistry. The characteristic hexagonal shape of sulfate green rust and the trapezoidal copper crystals were also identified on surface SEM images, further supporting the formation of these mineral phases and the XRD results (Fig. 4a). EDS analysis showed the presence of S and O, suggesting the occurrence of SO_4^{2-} anions at the surface and/or in the interlayer of the sulfate green rust formed. A bulbous formation of mixed iron (oxy)hydroxides aggregates due to increased iron corrosion was also observed on the surface of waste iron particles in the reactive zone.

Study of the reacted iron/sand surface with SEM revealed also several small (2–8 μm) scattered spheres (Fig. 4b). EDS analysis showed that these spheres are composed primarily of Fe and S with minor amounts of Ca, Si, and O. Therefore, these round grains are assumed to be precipitates of iron sulfide (or mackinawite), as indicated by XRD.

3.2. Effect of sand

In field-scale PRB applications, sand or gravel are generally mixed with reactive iron chips and used both as admixing and/or backfill material in subsurface trenches. This cost-effective design helps groundwater flow distribution through the PRB unit, minimizes both mineral precipitation and fouling at reactive surface sites, and therefore enhances PRB reactivity and lifetime. Although little is yet known about the spatial distribution of silica species within an iron-sand reactive zone and with regard to iron corro-

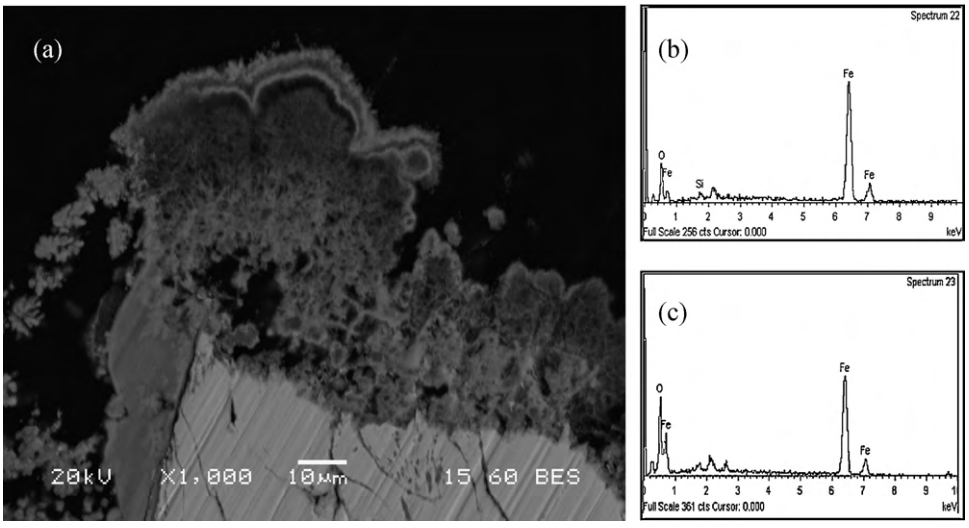

Fig. 3. (a) Cross sectional (SEM)–backscatter electron (BSE) image of cemented iron filings showing Fe (oxy)hydroxides corrosion coating adjacent to the iron filing surface, (b) and (c) representative EDS analyses of the iron coating shell.

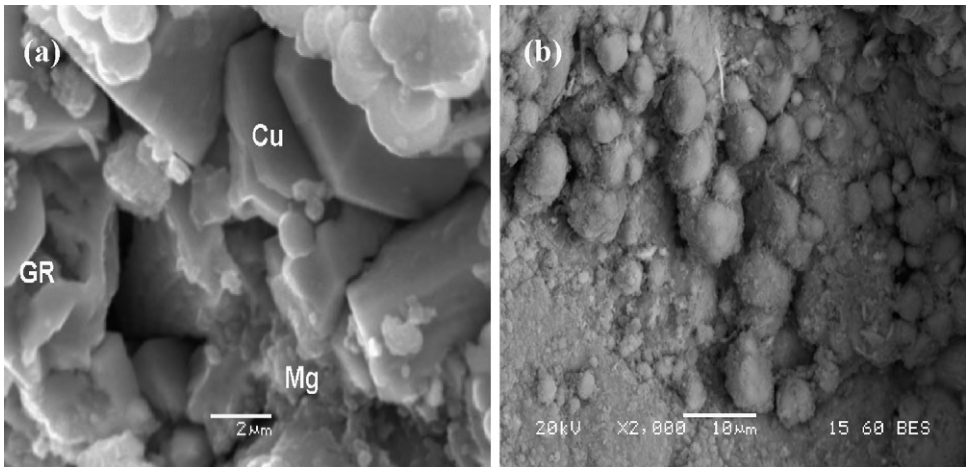

Fig. 4. Minerals present on the surface of a reacted iron filing: (a) SEM photomicrograph showing hexagonal-shaped green rust (GR), trapezoidal crystals of elemental copper (Cu) and formation of magnetite/maghemite aggregates onto iron surface (Mg). (b) SEM–BSE photomicrograph showing the distribution of rounded formations of FeS.

sion, recent studies have shown that dissolution of silica may limits system efficiency [42,43].

In natural waters, silica species are ubiquitous aqueous compounds that mainly occur as silicic acid ($Si(OH)_4$) through a single break of siloxane bonds (≡Si–O–Si≡) via water. Significant amounts of dissolved silica are also commonly encountered in mine effluents as a result of weathering of aluminosilicate minerals at low pH conditions. In this case, the overall dissolution reaction is monitored by the production of silicic acid, $H_4SiO_4(aq)$, as a final product of the congruent dissolution of $(am)SiO_2$ into water:

$$am\,SiO_2 + 2H_2O \Rightarrow H_4SiO_4(aq) \quad (6)$$

Overall, dissolution rates of $(am)SiO_2$ differ under standardized conditions, when normalized to mineral surface area. At pH 3 and 25 °C, $(am)SiO_2$ dissolution rate calculated by PHREEQC was found to be about 2.8×10^{-13} mol m^{-2} s^{-1}. However, the most noticeable feature is that the log of the dissolution rates varies almost linearly with pH above and below the minimum rate seen at pH 3 (Fig. 5). Similar dissolution rates of silica complexes were also determined using iron/sand mixtures in batch, column, and field investigations [44].

Although some researchers argue that dissolved silica promotes Fe^0 corrosion reaction by releasing protons in the solution through interaction with iron oxyhydroxide surface [45,46], recent studies have revealed its inhibitory effect on zero-valent iron reactivity over time [42,43]. In this study, three main distinct regions are

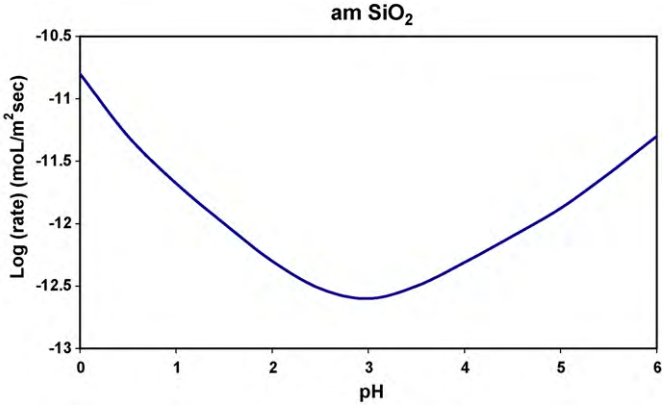

Fig. 5. Log rate dissolution of $amSiO_2$ as a function of pH.

observed by using SEM on polished sections of reacted iron-sand grains (Fig. 6a): the surface of the iron (Layer A), a dark brown non-porous crust corresponding to silica sand (Layer B) and a powdery layer of loosely bound, greyish Fe–Si precipitates (Layer C).

EDS point analyses showed that the iron grain in Layer A contains about 1.3% Si, whereas the aggregated Fe–Si precipitates (Layer C) contain almost 13.3% Si and traces of Ca (Table 2). Moreover, EDS analysis combined with 2D mapping (Fig. 6b–e) confirmed the penetration effect of Si into the iron coating shell; therefore, it is likely that a fraction of iron corrosion is promoted by its association with silica, thus creating a Fe–Si coating layer that potentially isolates pore water from the bulk flow. Oxygen signals occur adjacent to iron corrosion products in the filled pores, indicating the formation of iron oxyhydroxide layers while the scattered clusters of manganese at certain locations indicate a delayed sequence of its sulfide formation.

Silica/iron precipitates can either physically block access of the metals to the reactive sites, or they could chemically alter the reactivity of the interfacial region by changing the speciation of the surface-associated iron. Geochemical modelling calculations showed that the adsorption of dissolved silica onto the surface of iron fillings is likely to be manifested at high pH as solubility of silica increases with pH. The decrease in iron reactivity could be also explained by the tendency of silica to serve either as an anodic corrosion inhibitor that prevents iron from releasing electrons to the metal contaminants or as chemical converter that changes the types of iron (hydr)oxide phases that may be formed. A previous iron-sand column study conducted for the treatment of organohalides showed that the inhibitory effect of silica sand is not only dependent on the concentration of dissolved silica species in the feed solution, but also on the type of iron used in the reactive matrix [42].

Finally, it is important to note that anaerobic corrosion of waste iron by water would be expected to occur uniformly throughout the reactive zone in an iron-sand column system. However, exten-

Table 2
Distribution of elements at representative points in the regions of the waste iron, silica sand and Fe–Si precipitates.

EDS point at	Elements			
	Fe	Si	Ca	O
Layer A – waste iron	98.70	1.3	–	–
Layer B – silica sand	–	55.92	–	44.08
Layer C – silica/iron gel	59.89	13.31	0.61	26.19

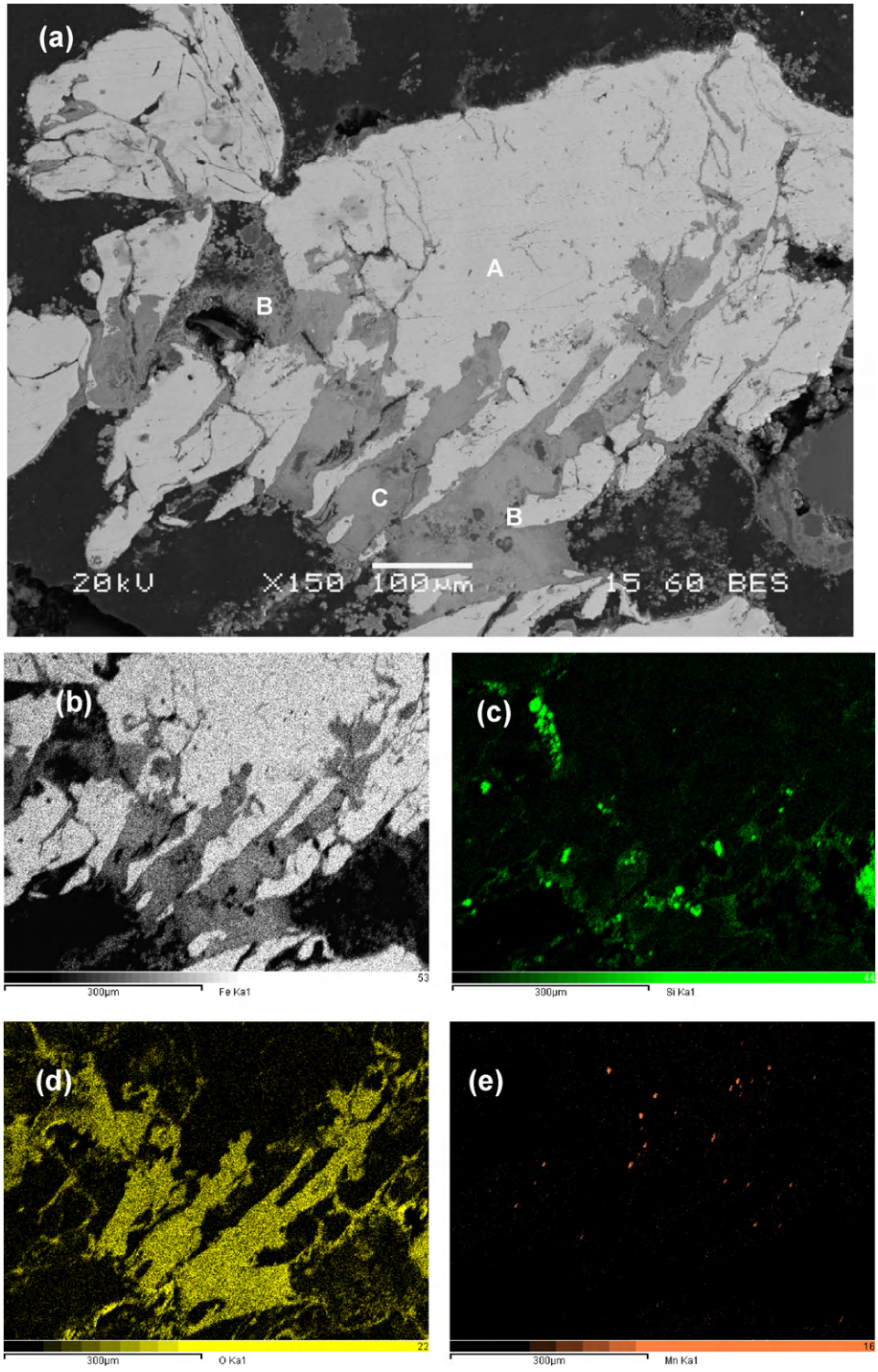

Fig. 6. SEM image of a polished cross section of a reacted iron-sand grain showing spatial relationship between iron filings (A), silica sand grains (B) and Fe–Si precipitates (C), and 2D mapping distribution of (b) Fe, (c) Si, (d) O and (e) Mn in this reference region.

sive surface cracking mainly due to iron corrosion was observed in selective grains of iron, with networks of cracks forming a series of distinct intercalated flakes, often linked by bridging spheroids. Cracks of approximately 500 μm in width and up to approximately 250 μm in length were observed on iron sections indicating that high iron corrosion rate prevailed during column operation. Similar signs of degeneration were also observed in field applications of iron barriers [28,47].

4. Conclusions

The overall results derived from this study suggest that PRBs filled with a reactive mixture of waste iron and sand can be used for cost-effective clean-up of acidic leachates.

Solid phase studies of the reactive mixture carried out at the end of column run with XRD, SEM/EDS and FTIR confirm the formation of new mineral phases (green rust, elemental copper, amorphous

iron sulfide and/or mackinawite) as well as the formation of iron (oxy)hydroxides (magnetite/maghemite, goethite) as a result of iron corrosion. Geochemical modelling is also required to fully understand chemical reactions in waste iron PRBs, including terms issues related with inhibition as well as with acceleration of corrosion and metal removal capacity.

Finally, both solid phase studies and geochemical modelling showed that although the dissolution of silica sand and concentration of sulfates can enhance metal removal by inducing the formation of iron (hydr)oxide and intermediate green rust particles, these particles in turn may affect the longevity of an iron PRB by deposition and filling of the pores. This could eventually reduce the porosity of the reactive zone, and thereby block the flow path and reduce the efficiency of a PRB. Therefore, the effects of sulfate and silica sand should be also taken into consideration when designing an iron PRB in the field.

References

[1] A. Kontopoulos, K. Komnitsas, A. Xenidis, N. Papassiopi, Environmental characterisation of the sulphidic tailings in Lavrion, Miner. Eng. 8 (10) (1995) 1209–1219.
[2] USEPA, A Citizen's Guide to Permeable Reactive Barriers (PRBs), EPA/542/F-01-005, 2001.
[3] P. Wanaratna, C. Christodoulatos, M. Sidhoum, Kinetics of RDX degradation by zero-valent iron (ZVI), J. Hazard. Mater. 136 (2006) 68–74.
[4] M.J. Lindsay, C.J. Ptacek, D.W. Blowes, W.D. Gould, Zero-valent iron and organic carbon mixtures for remediation of acid mine drainage: batch experiments, Appl. Geochem. 23 (8) (2008) 2214–2225.
[5] C. Noubactep, G. Meinrath, P. Dietrich, M. Sauter, B.J. Merkel, Testing the suitability of zerovalent iron materials for reactive walls, Environ. Chem. 2 (1) (2005) 71–76.
[6] C. Noubactep, A critical review on the process of contaminant removal in Fe^0-H_2O systems, Environ. Technol. 29 (8) (2008) 909–920.
[7] K. Komnitsas, G. Bartzas, I. Paspaliaris, Efficiency of limestone and red mud barriers: laboratory column studies, Miner. Eng. 17 (2004) 183–194.
[8] K. Komnitsas, G. Bartzas, I. Paspaliaris, Hydraulic performance of laboratory PRBs for the decontamination of acidic mine waters, in: J. Loredo, F. Pendás (Eds.), Proceedings of IMWA'05 – 9th International Mine Water Association Congress, September 5–7, Oviedo, Spain, 2005, pp. 347–354.
[9] J. Wantanaphong, S.J. Mooney, E.H. Bailey, Suitability of natural and waste materials as metal sorbents in permeable reactive barriers (PRBs), Environ. Chem. Lett. 3 (2005) 19–23.
[10] C. Noubactep, The suitability of metallic iron for environmental remediation, Environ. Prog., doi:10.1002/ep.10406 (2010).
[11] J.S. Ahn, C.M. Chon, H.S. Moon, K.W. Kim, Arsenic removal using steel manufacturing byproducts as permeable reactive materials in mine tailing containment systems, Water Res. 37 (2003) 2478–2488.
[12] G. Bartzas, K. Komnitsas, I. Paspaliaris, Laboratory evaluation of Fe^0 barriers to treat acidic leachates, Miner. Eng. 19 (2006) 505–514.
[13] Y. Wu, R. Versteeg, L. Slater, D. LaBrecque, Calcite precipitation dominates the electrical signatures of zero valent iron columns under simulated field conditions, J. Contam. Hydrol. 106 (3–4) (2009) 131–143.
[14] M.S. Odziemkowski, T.T. Schuhmacher, R.W. Gillham, E.J. Reardon, Mechanism of oxide film formation on iron in simulating groundwater solutions: Raman spectroscopic studies, Corros. Sci. 40 (1998) 371–389.
[15] T.E. Shokes, G. Möller, Removal of dissolved heavy metals from acid rock drainage using iron metal, Environ. Sci. Technol. 33 (1999) 282–287.
[16] Y. Roh, S.Y. Lee, M.P. Elless, Characterization of corrosion products in the permeable reactive barriers, Environ. Geol. 40 (2000) 184–194.
[17] T.C. Zhang, Y.H. Huang, Profiling iron corrosion coating on Fe^0 grains in a zero-valent iron system under the influence of dissolved oxygen, Water Res. 40 (12) (2006) 2311–2320.
[18] J.F. Devlin, J. Klausen, R.P. Schwarzenbach, Kinetics of nitroaromatic reduction on granular iron in recirculating batch experiments, Environ. Sci. Technol. 32 (13) (1998) 1941–1947.
[19] Y. Zhang, R.W. Gillham, Effects of gas generation and precipitates on performance of Fe0 PRBs, Ground Water 43 (2005) 113–121.
[20] S.W. Jeen, R.W. Gillham, D.W. Blowes, Effects of carbonate precipitates on long-term performance of granular iron for reductive dechlorination of TCE, Environ. Sci. Technol. 40 (2006) 6432–6437.
[21] D.I. Kaplan, T.J. Gilmore, Zero-valent iron removal rates of aqueous Cr(VI) measured under flow conditions, Water Air Soil Pollut. 155 (2004) 21–33.
[22] K. Komnitsas, G. Bartzas, I. Paspaliaris, Inorganic contaminant fate assessment in zero-valent iron treatment walls, Environ. Forensics 7 (2006) 207–217.
[23] K. Komnitsas, G. Bartzas, I. Paspaliaris, Modeling of reaction front progress in fly ash permeable reactive barriers, Environ. Forensics 7 (2006) 219–231.
[24] K. Komnitsas, G. Bartzas, K. Fytas, I. Paspaliaris, Long-term efficiency and kinetic evaluation of ZVI barriers used for clean up of copper containing solutions, Miner. Eng. 20 (2007) 1200–1209.
[25] D.L. Parkhurst, C.A.J. Appelo, User's guide to PHREEQC (version 2): a computer program for speciation, batch reaction, one dimensional transport, and inverse geochemical calculations, US Geological Survey Water Resources Investigations, 1999, pp. 99–4259.
[26] J.W. Ball, D.K. Nordstrom, WATEQ4F—User's manual with revised thermodynamic data base and test cases for calculating speciation of major, trace and redox elements in natural waters, US Geological Survey open file report, 1991, pp. 90–129.
[27] P.S Sidhu, R.J. Gilkes, A.M. Posner, Mechanism of the low temperature oxidation of synthetic magnetites, J. Inorg. Nucl. Chem. 39 (1977) 1953–1958.
[28] Y. Furukawa, J.W. Kim, J. Watkins, R.T. Wilkin, Formation of ferrihydrite and associated iron corrosion products in permeable reactive barriers of zero valent iron, Environ. Sci. Technol. 36 (2002) 5469–5475.
[29] M. Koschorreck, K. Wendt-Potthoff, W. Geller, Microbial sulfate reduction at low pH in sediments of an acidic lake in Argentina, Environ. Sci. Technol. 37 (2003) 1159–1162.
[30] A.H.M. Hulshof, D.W. Blowes, W.D. Gould, Evaluation of in situ layers for treatment of acid mine drainage: a field comparison, Water Res. 40 (2006) 1816–1826.
[31] J.L. Jambor, M. Raudsepp, K. Mountjoy, Mineralogy of permeable reactive barriers for the attenuation of subsurface contaminants, Can. Mineral. 43 (2005) 2117–2140.
[32] D.H. Dvorak, R.S. Hedin, H.M. Edenborn, P.E. McIntire, Treatment of metal-contaminated water using bacterial sulfate reduction: results from pilot-scale reactors, Biotechnol. Bioeng. 40 (5) (1992) 609–616.
[33] R.L. Parfitt, R.C. Smart, The mechanism of sulfate adsorption on iron oxides, Soil Sci. Soc. Am. J. 42 (1978) 48–50.
[34] R.T. Wilkin, M.S. McNeil, Laboratory evaluation of zero-valent iron to treat water impacted by acid mine drainage, Chemosphere 53 (2003) 715–725.
[35] C. Su, R.W. Puls, Significance of iron (II, III) hydroxycarbonate green rust in arsenic remediation using zerovalent iron in laboratory column tests, Environ. Sci. Technol. 38 (2004) 5224–5231.
[36] R.L. Frost, J.T. Kloprogge, Z. Ding, The Garfield and Uley nontronites—an infrared spectroscopic comparison, Spectrochim. Acta Part A 58 (2002) 1881–1894.
[37] S. Musić, M. Gotić, S. Popović, X-ray diffraction and Fourier transform-infrared analysis of the rust formed by the corrosion of steel in aqueous solutions, J. Mater. Sci. 28 (1993) 5744–5752.
[38] S. Peulon, L. Legrand, H. Antony, A. Chausse, Electrochemical deposition of thin films of green rusts 1 and 2 on inert gold substrate, Electrochem. Commun. 5 (2003) (2003) 208–213.
[39] M.H. Sousa, F.A. Tourinho, J.C. Rubim, Use of Raman micro-spectroscopy in the characterization of $MIIFe_2O_4$ (M = Fe, Zn) electric double layer ferrofluids, J. Raman Spectrosc. 31 (3) (2000) 185–191.
[40] I.N. Bhattacharya, P.K. Gochhayat, P.S. Mukherjee, S. Paul, P.K. Mitra, Thermal decomposition of precipitated low bulk density basic aluminium sulphate, Mater. Chem. Phys. 88 (2004) 32–40.
[41] A. Muramatsu, K. Kanie, Mechanistic study on formation of iron hydroxides and oxides with FT-IR and UV photospectroscopy, in: Y. Waseda, S. Suzuki (Eds.), Characterization of Corrosion Products on Steel Surfaces, Springer, Berlin, 2006, pp. 51–76.
[42] T. Kohn, L. Roberts, The effect of silica on the degradation of organohalides in granular iron columns, J. Contam. Hydrol. 83 (1–2) (2006) 70–88.
[43] E. Bi, J.F. Devlin, B. Huang, Effects of mixing granular iron with sand on the kinetics of trichloroethylene reduction, Ground Water Monitor. R. 29 (2) (2009) 56–62.
[44] R.M. Powell, R.W. Puls, Proton generation by dissolution of intrinsic or augmented aluminosilicate minerals for in situ contaminant remediation by zero-valence-state iron, Environ. Sci. Technol. 31 (1997) 2244–2251.
[45] T.D. Mayer, W.M. Jarrell, Assessing colloidal forms of phosphorus and iron in the procedures to polluted and unpolluted soils, Science Total Environ. 178 (1–3) (1996) 37–44.
[46] O.X. Leupin, S.J. Hug, Oxidation and removal of arsenic (III) from aerated groundwater by filtration through sand and zero-valent iron, Water Res. 39 (9) (2005) 1729–1740.
[47] D.H. Phillips, B. Gu, D.B. Watson, Y. Roh, L. Liang, S.Y. Lee, Performance evaluation of a zero-valent iron reactive barrier: mineralogical characteristics, Environ. Sci. Technol. 34 (2000) 4169–4176.